Vanadium oxide coatings to self-regulate current sharing in high-temperature superconducting cables and magnets

Zhenghuai Yang[1,2,a)], Aurora Cecilia Araujo Martínez[1,3], Sachin V. Muley[1,4], Xiaorong Wang[1], Qing Ji[1,a)], André Anders[1,5,6]

1. Lawrence Berkeley National Laboratory, 1 Cyclotron Road, Berkeley, CA 94720, U.S.A.
2. National Key Laboratory of Science and Technology on Advanced Composites in Special Environments, Harbin Institute of Technology, Harbin 150080, P. R. China
3. Division of Sciences and Engineering, Leon Campus, University of Guanajuato, Loma del Bosque 103, Lomas del Campestre, 37150, Leon, Guanajuato, Mexico
4. Department of Materials Science and Engineering, University of Wisconsin-Madison, 1509 University Avenue, Madison, WI 53706, U.S.A.
5. Leibniz Institute of Surface Engineering (IOM), Permoserstr. 15, 04318 Leipzig, Germany
6. Leipzig University, Faculty of Physics and Earth Sciences, Linnéstraße 5, 04103 Leipzig, Germany

a) Corresponding Authors:
Zhenhuai Yang (Email: yzh_hh@163.com);
Qing Ji (Email: qji@lbl.gov)

Please cite this article as Zhenghuai Yang, Aurora Cecilia Araujo Martínez, Sachin V. Muley, Xiaorong Wang, Qing Ji, and André Anders. 2020. "Vanadium Oxide Coatings to Self-Regulate Current Sharing in High-Temperature Superconducting Cables and Magnets." Journal of Applied Physics 128 (5): 055105.
https://doi.org/10.1063/5.0013783.

Abstract

High-temperature superconductors such as $REBa_2Cu_3O_{7-\delta}$ (REBCO, RE = rare earth) enable high-current cables and high-field magnets. By removing the turn-to-turn insulation in a magnet application, recent experiments demonstrated that REBCO magnets can self-protect against catastrophic damage during a superconducting-to-normal transition (quench), i.e. when the stored magnetic energy rapidly converts to heat. The current can bypass the hot spot during a quench, thereby reducing the localized heat dissipation. The removal of the insulation between turns, however, leads to excessive eddy currents during current ramping, thereby forcing a much-prolonged magnet charging time. To address this issue, we investigate vanadium oxide (VO_x) coatings as a temperature-dependent self-switching medium that automatically manages current sharing. VO_x coatings (with $1.70 \leq x \leq$ to 2.07) were deposited by reactive cathodic arc deposition, initially on insulating glass to determine the electrical properties, and later on commercial REBCO tapes. The coatings are X-ray amorphous but with short-range crystalline ordering according to Raman spectrometry. The resistivity of VO_x decreased by at least three orders of magnitude when the temperature increased from 80 to 300 K. The coating process is compatible with commercial REBCO tapes as evidenced by the negligible change of the critical current caused by the coating process. The results from current sharing experiments and circuit analysis suggest that the VO_x coating can effectively self-regulate current sharing in REBCO magnets, suppress excessive eddy currents and enable self-protection during quenches.

1. Introduction

Vanadium oxides (VO_x) can occur in many phases and offer rich physics with their complex crystal structures and electronic properties. They also occur in so-called Magnéli phases defined by the general stoichiometric formula.[1]

$$V_nO_{2n-1} = V_2O_3 + (2n\text{-}1)\ VO_2$$

where $2 \leq n \leq 9$ or $n \rightarrow \infty$.

They are well known because they can undergo a metal-insulator transition (MIT) with a change in temperature,[2,3] except for V_7O_{13}. VO_2 is by far the most common and most investigated among the vanadium oxides since the MIT occurs just marginally above room temperature (~68°C) suggesting applications for thermochromic windows,[4-7] and electrical switching devices.[8] Research on other phases is limited because their transition temperatures are in the cryogenic region, namely V_2O_3 (158 K), V_5O_9 (135 K), V_6O_{11} (170 K) and V_8O_{15} (70 K).[9] Interestingly, VO_2, whose resistance also gradually decreases orders of magnitude when lowering the temperature to ~100 K from room temperature, however is rarely studied at low temperature likely due to a perceived lack of applications. So far, apart from window applications, most applications of these MIT materials are in memory devices or energy storage.[10,11] Application of the resistance change property induced by low temperature thermal resistor devices might be promising but the transition hysteresis needs to be eliminated.[1]

A new field of application of VO_x may be in high-temperature superconducting (HTS) magnets, which are needed in the next generation of hadron colliders, in proton and carbon therapy,[12] compact fusion reactors, NMR magnets, and next generation electric motors and generators.[13-19] Of particular interest are $REBa_2Cu_3O_{7-\delta}$ (RE = rare earth, REBCO) coated conductors featuring a high irreversibility field (the magnetic field at which the bulk critical current density goes to zero) and high critical current density over a wide temperature, e.g., between 4.2 K (liquid helium) and 20 K (liquid hydrogen).

The protection of superconducting magnets against quench (a transition from superconducting to normal-conducting state) poses a significant challenge because the high magnetic energy stored in superconducting coils converts into heat during quench. The heat of the conductor winding, if not removed from or distributed uniformly inside the coil, can cause catastrophic damage to the magnets.[20] Quench protection becomes even more challenging for HTS magnets because the hot spots do not propagate as fast as in the low-temperature superconducting magnets.[21]

Recent single pancake coils with no electrical insulation between REBCO tapes demonstrate the possibility of self-protection during fault conditions by allowing the current to bypass the hot spot and share into the neighboring conductors through the turn-to-turn contact during a quench, which reduces the heat generation and the risk of coil damage.[22] The non-insulation approach, however, leads to excessive eddy currents inside the coil due to the low electrical resistance between tapes and changing magnetic field during current ramping.[22,23] The eddy currents significantly distort the magnetic field generated by the coil and increases the magnet energization time required to reach the design field.[24,25] These behaviors can become an issue for applications such as particle accelerator magnets and high-field fusion reactor magnets.

Increasing the electrical resistance between the tapes can effectively reduce the eddy currents, which is demonstrated by co-winding REBCO tapes with resistive strips.[26] Lu *et al.* coated REBCO tapes with resistive films such as Ni and Cr and oxidized the surface of REBCO tape with a commercial copper blackening agent.[27] The current sharing between tapes, however, may be hindered by the increased turn-to-turn electrical resistance.

A potential solution to address this problem is to coat the REBCO conductors with a temperature-regulated passive medium whose electrical resistance decreases with increasing temperature. When a local hot spot appears during a quench, the electrical resistance of the coating becomes low enough to allow current sharing. At

the operation temperature, the resistance is high to suppress the eddy currents between turns during the current ramping. This approach has the potential to enable reliable protection of REBCO cables and magnets against fault conditions without compromising the field quality or ramping time required for various magnet applications.

Kim *et al*.[28,29] directly painted V_2O_3 powders on HTS conductors and demonstrated the advantage of this self-switching resistance layer. Compared with a layer from powders, thin films made by physical vapor deposition (PVD) can be advantageous in terms of the adjustable resistance properties and industrial production. However, previous growth condition for VO_x films required high temperature, usually above 300 °C, which may damage the REBCO conductors.[30-32] Therefore, a method to deposit VO_x coatings compatible with the REBCO conductors is of great interest for applications in HTS cables and magnets.

In this work, VO_x coatings were deposited on commercial REBCO tapes by reactive cathodic arc deposition,[33] a technique that can keep the substrate temperature low during the coating process. We will show that the resistivity of VO_x coatings increases by orders of magnitude when decreasing the temperature from room temperature to around 77 K. We will also show an experimental demonstration of current bypassing a local heat-induced quench zone on HTS tape and flowing through the neighboring conductor, and present an electric circuit model to understand the impact of VO_x coating on the current sharing characteristics for future applications in REBCO cables and magnets.

2. Experiments

2.1 Coating deposition and characterization

VO_x coatings were deposited on glass substrates and REBCO tapes by a cathodic arc system as shown in Fig.1. We used 4 mm wide and 120 mm long commercial REBCO tapes from SuperPower Inc. These tapes are produced in an automated process where ~ 1 μm YBCO layer is grown on a 50 μm thick Hastelloy substrate and

a series of buffer layers. A 2 μm silver overlayer is added and a copper surrounding layer is electroplated as stabilizer.[34] Two kinds of tapes were used: one has a 40 μm thick Cu stabilizer and the other has a 100 μm thick Cu stabilizer.

A vanadium cathode of 99.9% purity was used in the arc deposition experiment. Vanadium plasma was generated using a DC arc power supply with an open circuit voltage of 160 V and an operating current of 65 A. A coil with a DC-current of 95 A guided the plasma from the cathode to the REBCO tapes (Fig. 1).[33] The plasma transport coil has the additional function of partially dissociating and ionizing the oxygen background through interaction with magnetized electrons of the vanadium plasma. The VO_x compound coating is formed on the REBCO tape when the flux of vanadium deposits and reacts with oxygen.

The REBCO tape was mounted on a holder that periodically moved back and forth during the deposition such as to coat on a larger area and to avoid excessive local heating on the REBCO tape caused by the deposition process. The tape holder was electrically floating to prevent the REBCO tape from becoming part of the arc discharge circuit. The peak temperature on the REBCO tape was measured to be lower than 100 ℃ during the coating process.

The stoichiometry of the coatings can be adjusted through the vanadium flux, the oxygen partial pressure and oxygen activation (dissociation and ionization) in the plasma transport coil. The most straightforward process control parameter is the oxygen flow, which was varied between 20 and 28 sccm while the argon flow was fixed at 25 sccm. The purpose of argon was to help maintain the stability of the arc discharge.

Chemical compositions of the deposited coatings were characterized by Rutherford Backscattering Spectrometry (RBS) using a 2 MeV helium ion beam. Raman spectra were recorded using a Horiba Jobin Yvon LabRAM system with a 532 nm laser. Electrical resistivity of the coating on glass substrates was measured from 80 to 300 K in steps of 5 K with an Ecopia HMS-5000 Hall measurement system with

a 0.55 T background magnetic field.

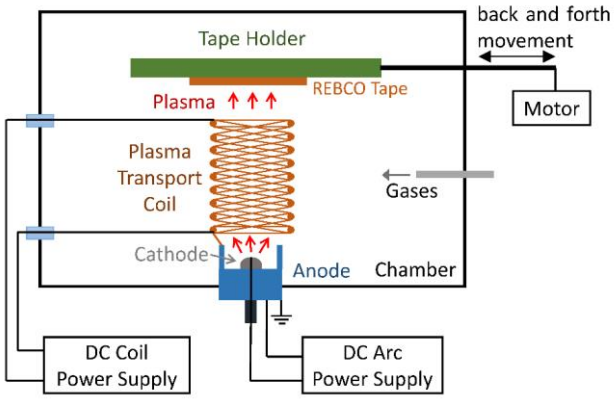

Fig. 1 Diagram of the cathodic arc deposition system.

2.2 Experimental setup and measurement protocols to study the impact of VO_x coatings on REBCO tapes

We performed the following three experiments to study the impact of the VO_x coatings on REBCO tapes:

1) Using a cryostat, measure the current-carrying capability of REBCO tapes at 77 K before and after coating to verify whether the coating process degraded the tape.

2) Measure the electrical resistance of the VO_x coating between two REBCO tapes in a lap-joint configuration as a function of temperature.

3) Measure the impact of VO_x coating on the current-sharing behavior.

2.2.1 Impact of the coating process on the current-carrying capability of REBCO tape

The critical current (I_c) of a 120 mm long REBCO tape before and after coating was measured in liquid nitrogen at 77 K with the self-magnetic field generated by the transport current in the tape. A pair of voltage taps, 30 mm apart, was soldered to the REBCO tape using Sn60Pb40 solder. Both ends of the tape were soldered to the current leads. The sample holder was submerged in liquid nitrogen during the test. We applied a DC current to the REBCO tape in steps of few amperes and measured the voltage with a Keithley 2182A nanovoltmeter. The power supply was shut off when the voltage across the REBCO tape reached 10 μV. To determine the critical current I_c

and *n* values of the REBCO tape, the measured voltage-current data were fitted to the power law,

$$E = E_c \left(\frac{I}{I_c} \right)^n , \quad (1)$$

where E_c is the electrical field of 1 μV cm^{-1} that we use to define the I_c.[21]

2.2.2 Lap-joint configuration to measure the resistivity of the VO_x coating between two REBCO tapes

To measure the electrical resistance of the VO_x coatings on actual REBCO-tape as opposed on glass substrates, we measured the resistance across a lap joint between two REBCO tapes with near-zero I_c with a four-probe method. One tape has the VO_x coating deposited at an oxygen flow rate of 24 sccm and the other tape has no coatings. Both tapes were pressed against each other (Fig. 2) using the setup described in the next section. An electrical insulating sheet was used to form a contact area of about 4 mm^2 between two tapes. A constant current of 10 mA was applied from the top to bottom tape during the test. The voltage across the lap joint was measured continuously when the setup was cooled down from room temperature to 77 K. For comparison, we repeated the measurements with tapes without the VO_x coating.

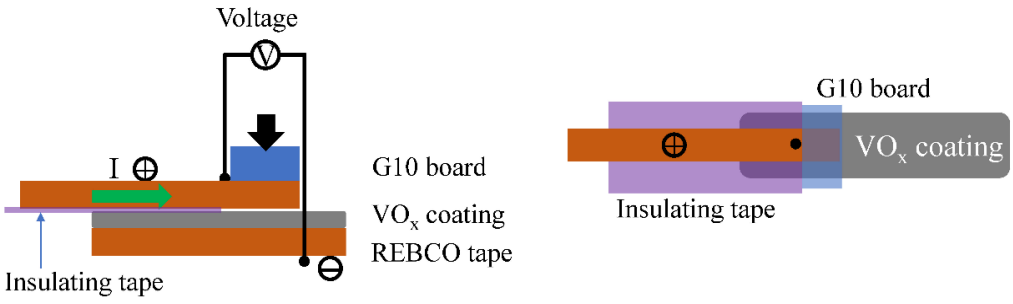

Fig. 2 Sketch (not to scale) for the lap joint experiment between two REBCO tapes with the VO_x coating in between. Left: side view. Right: top view.

2.2.3 Impact of the coating on the current sharing behavior of REBCO tape

An experimental setup was developed to measure the impact of the VO_x coating on the current sharing behavior between a REBCO tape and a Cu strip (Fig. 3). Thirteen spring loaded contact pins measured the voltage across 12 consecutive

sections along the REBCO tape with each section 6 mm long. The voltage across each pair of pins was measured using a Keithley 2182A nanovoltmeter. Three heaters made from NiCr wires were embedded and sealed with Stycast 2850 FT in the sample holder (H1 to H3 in Fig. 3). Each heater has a resistance of 1.3 Ω at room temperature. A type-E thermocouple was also embedded under each heater to monitor the heater temperature. The heater was powered by an HP6033A power supply controlled by a LabView program via a GPIB bus. A Cu strip was placed on top of the VO_x coating to detect the current sharing and to protect the coating from possible damage by the spring-loaded pins. This setup allowed to mount and dismount REBCO tapes and to improve the reproducibility of the experiments. During the measurements, the sample holder was immersed in liquid nitrogen bath. REBCO tapes were tested both before and after coating.

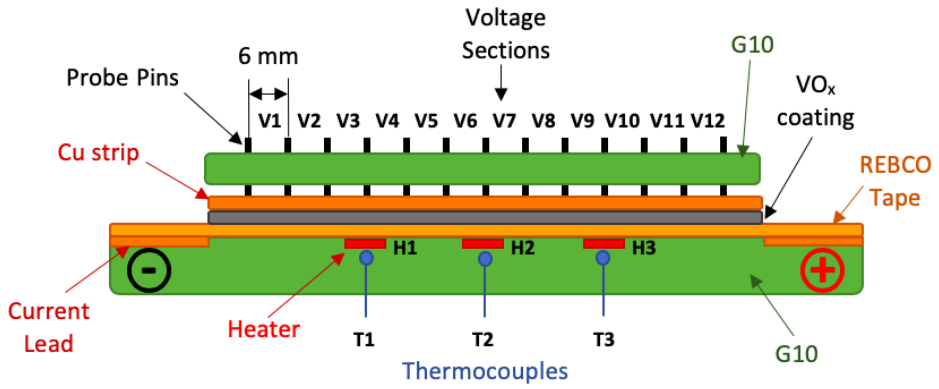

Fig. 3 Schematic diagram of the experimental setup (front view not to scale) to study the impact of VO_x coating on current sharing in REBCO tapes.

Two sets of measurements were performed. One set was similar to the critical current measurements as described in 2.2.1 where the temperature of the REBCO tapes remained at 77 K. The REBCO tape used in this experiment had a 40 µm thick Cu stabilizer, I_c of 95 A, and *n*-value of 32. The Cu strip placed on top of the REBCO tape was 1 mm thick, 3 mm wide and 100 mm long.

The other set of measurements was performed to demonstrate current sharing when a local hot spot was induced by the Heater H2 (Fig. 3). Since we ran out of the

earlier REBCO tapes, a REBCO tape with a 100 μm thick Cu stabilizer with a similar I_c and n values was used. We covered the sample holder with solder flux along Sections V4 to V10 to reduce the thermal contact between the REBCO tape, Cu strip and liquid nitrogen. To increase the peak temperature during a heater-induced quench, we reduced the thickness of the Cu strip from 1 to 0.29 mm. During the measurement, a constant transport current ($I_{transport}$) of 80 A (82% of the I_c) was applied to the REBCO tape. Once the $I_{transport}$ stabilized, we ramped the voltage across Heater H2 from zero to 8.5 V to induce the quench of REBCO tapes.

2.3 Electric-circuit model to analyze the current sharing behavior in bare and coated REBCO tapes

An electric-circuit model was developed and analyzed via SPICE[35]-based simulation software (LTspice and NGSPICE) (Fig. 4).[36] Each tape section consists of a non-linear voltage source for the REBCO layer following equation (1), a resistance for the Cu stabilizer, transverse and longitudinal resistances for the VO_x coating, and a resistance for the Cu strip. The model also includes the contact resistance between the Cu strip and the VO_x coating. Perfect contact between the VO_x coating and the Cu stabilizer was assumed. The contact resistance was estimated to be around 550 μΩ based on a contact resistivity of 100 μΩ·cm^2 as reported in ref. 37. For the Cu resistances we used the electrical resistivity of Cu with a residual resistivity ratio of 50.

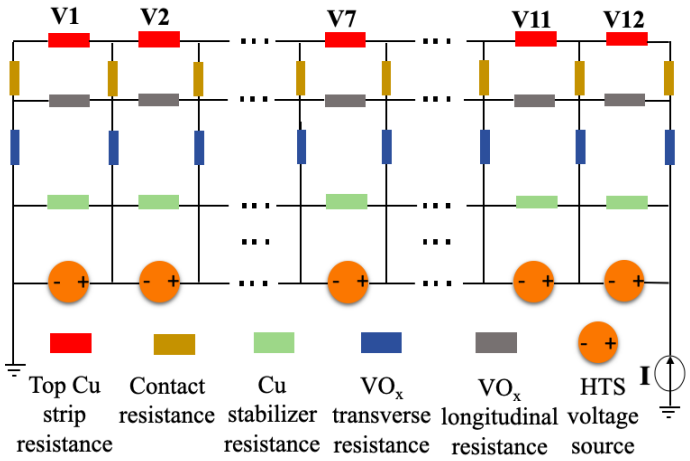

Fig. 4 Diagram of the electric-circuit model used for the simulations.

3. Results and Discussion

3.1 Chemical composition and thickness of the VO_x coatings

Chemical composition and thickness information of the VO_x coating were determined using Rutherford backscattering (RBS). A typical RBS spectrum of VO_x coating deposited on glass substrates with an oxygen flow rate of 20 sccm is presented in Fig. 5 (a). The peaks located at different channel numbers can be attributed to the elements of O (375), Na (450), Si (520), Ca (630), and V (755) respectively. Na, Si, Ca, and part of O belong to the glass substrate, V and part of O can be assigned to the coating. The element ratios and coating thicknesses can be obtained from a well-established fitting procedure using RBS raw data. The ratio of O/V can be determined by the intensities of element signal and corrected for the scattering cross sections of each element. The width of the V signal is directly proportional to the thickness of the VO_x layer. The O/V ratio and thickness with the different oxygen flow rates were presented in Fig. 5 (b). The O/V ratio was 1.70 at an oxygen flow rate of 20 sccm; it increased continuously to about 2.07 when the oxygen flow rate increased to 28 sccm. Coating thickness, as commonly expressed in RBS-measurements by atoms/cm^2, gradually decreased with the increase of the oxygen flow rate.

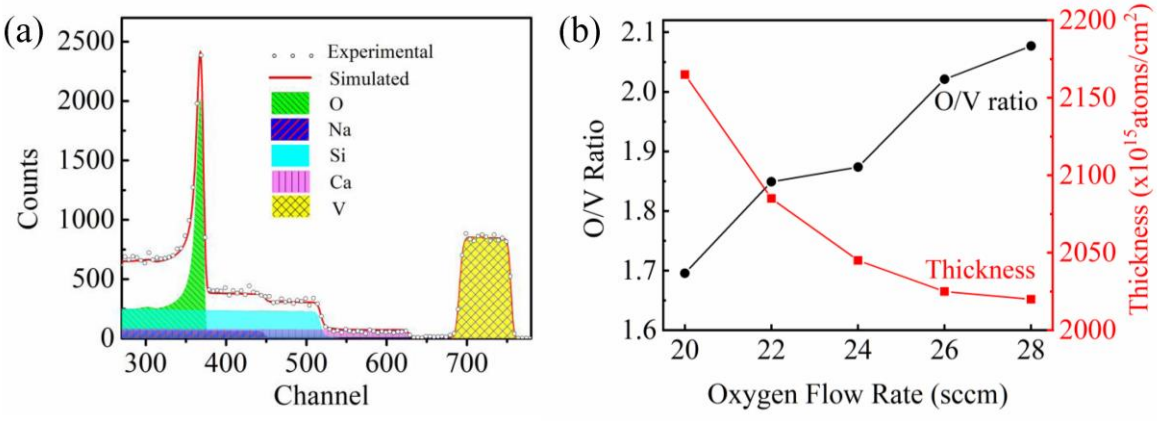

Fig. 5 (a) RBS spectrum of VO_x coating deposited on glass substrate; (b) O-V ratio and thickness distribution with different oxygen flow rate.

3.2 Microstructure of the VO_x coatings

The structures of the VO_x coatings deposited with different oxygen flow rates

were characterized by X-ray diffraction (XRD) and Raman spectrometry. The XRD spectra are shown in Fig. 6 (a): no crystallization peak can be detected from the XRD characterization, which means the coatings are X-ray amorphous. This is reasonable because the process heating was kept low during the deposition, and templating does not apply because our substrates were amorphous glass.

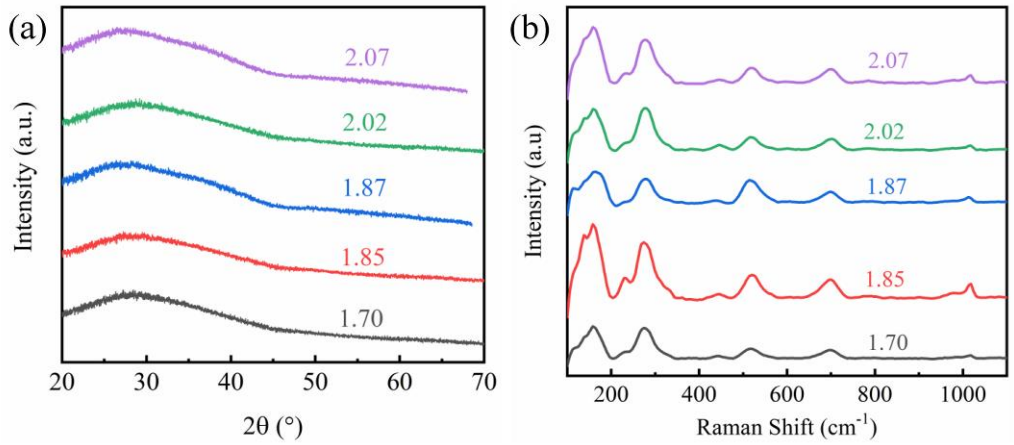

Fig. 6 (a) XRD and (b) Raman spectra of VO_x coatings with different O/V ratio deposited under the oxygen flow rates from 20 sccm to 28 sccm.

In the Raman spectra shown in Fig. 6 (b), the main peaks were located around 138, 158, 230, 275, 330, 445, 520, 700, 1020 cm^{-1}. All these peaks were broad and relatively low in intensity. Different peak positions can be attributed to the different phases of VO_x.[38-44] The Raman peaks at ~ 275 cm^{-1} and ~520 cm^{-1} can be assigned to the A_{1g} vibration modes of the high temperature metallic phase of a V_2O_3 thin film, while the peak at ~330 cm^{-1} is the phonon mode of E_g.[38] The broad peak at 443 cm^{-1} is related to magnon scattering in the anti-ferromagnetic phase of V_2O_3 thin film.[39] The peaks located at ~ 138 cm^{-1}, 700 cm^{-1}, and ~1020 cm^{-1} agree with the accepted peak position for a V_2O_5 film.[40-42] For the VO_2 films, the Raman vibrational modes are commonly located at ~158 cm^{-1}, 275 cm^{-1}, 445 cm^{-1} and ~520 cm^{-1}.[43,44] Based on previous publications and the coating parameters used in this work, it is reasonable to conclude that the VO_x films coated on glass substrates consisted of various phases of vanadium oxide. Although XRD analysis gave no indication of crystalline vanadium oxide, Raman study revealed the presence of crystallinity. This is due to the sensitivity

of Raman spectroscopy to short-range vibrational modes of bond configurations, while XRD responds to long-range order crystallinity of materials.[43] Hence, the observed behavior suggests that the samples are X-ray amorphous with a short-range crystalline ordering of different phases. If crystallization is necessary for the MIT transition, the coating process needs to be further optimized or the impact of higher deposition temperature needs to be studied.

3.3 Resistivity of the VO_x coating as a function of temperature

The electrical resistivity as a function of temperature for coatings deposited under different oxygen flow rates is presented in Fig. 7. The resistivity of VO_x coatings at 300 K was sensitive to oxygen conditions during the deposition. It increased by four orders of magnitude from ~0.01 to ~150 Ω·cm when the oxygen flow was increased from 20 to 28 sccm.

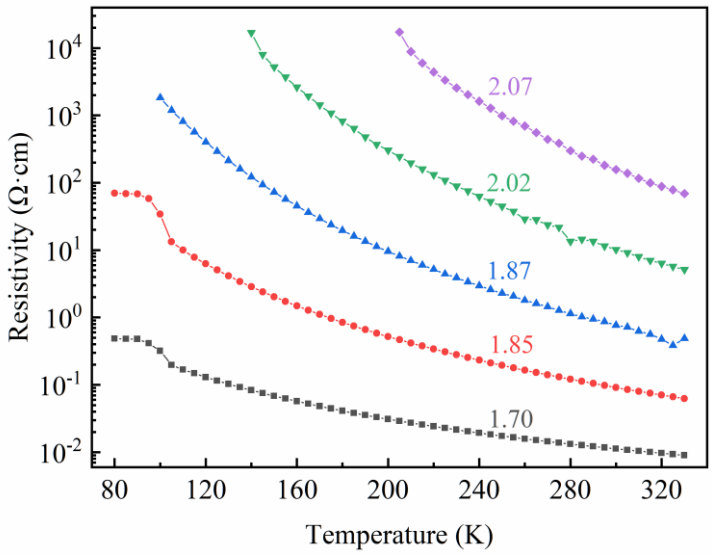

Fig. 7 Resistivity as a function of temperature for VO_x coatings with different O/V ratio deposited under the oxygen flow rates from 20 sccm to 28 sccm.

For the coatings fabricated at low oxygen flow (1.70 and 1.85 O/V ratio), as the temperature decrease from room temperature, the resistivity gradually increased followed by a relative abrupt increase observed around 100 K (Fig. 7). For the coatings deposited at high oxygen flow (1.87, 2.02, and 2.07 O/V ratio), the resistance at low temperature was beyond the measuring range of the equipment and no

transition was measured for those coatings.

We therefore have demonstrated that the VO_x coating is a promising candidate for the proposed mechanism to self-regulate current sharing between REBCO tapes since the measured resistivity covers the range from electrical conductors to insulators by controlling the oxygen flow rate during deposition. When the temperature increased, all the coatings showed a significant decrease in resistivity with orders of magnitude variation.

3.4 Effect of the VO_x coatings on REBCO tapes

3.4.1 Impact of the coating process on the current-carrying capability of REBCO tapes

Fig. 8 compares the electric field as a function of current of REBCO tapes measured before and after coating. I_c values before and after coating were 89.5 A and 88.6 A, and the *n* values were 34.2 and 33.8, respectively. Negligible changes in I_c and *n* values demonstrate that the coating process reported here preserves the current-carrying capability of the REBCO tape, necessary for the proposed application of the VO_x coating.

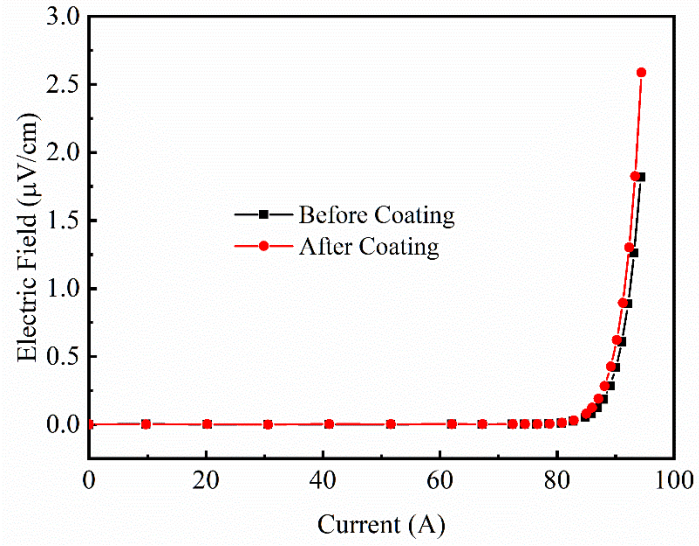

Fig. 8 The electric field as a function of current for the REBCO tape before and after the coating process. Measurements were performed at 77 K with the self-magnetic field generated by the transport current in the REBCO tape.

3.4.2 The resistivity of the VO_x coating on REBCO tapes measured from the lap-

joint configuration

The voltages measured in the lap-joint configuration are shown in Fig. 9. With the same injected current of 10 mA, without the VO_x coating, the voltage across two tapes decreased from ~170 μV to ~5 μV when the setup was cooled down from room temperature to 77 K. This is because the resistivity of copper decreases with temperature. With the VO_x coating, in contrast, the voltage increased from ~210 μV to ~12.5 mV because the resistivity of VO_x coating increased as the temperature decreases. The entire system shows a voltage difference by a factor of ~10^4 between the cases with and without coating at 77 K. The voltage drop across the VO_x layer increases from 40 μV at room temperature to roughly 12.5 mV at 77 K. Based on this, we calculated the VO_x resistivity change of a factor of around 300 between room temperature and 77 K. Thus, the resistivity of the VO_x coating was 1 Ω·cm at 300 K and 300 Ω·cm at 77 K, which is consistent with previous Hall effect measurements of the coatings deposited on glass substrates (Fig. 7).

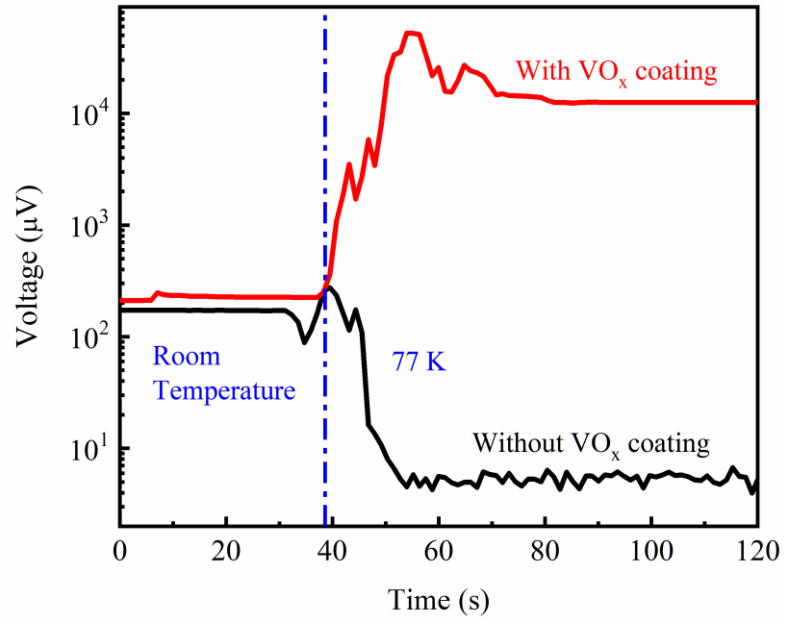

Fig. 9 Measured voltage in the lap-joint configuration at room temperature and 77 K for the cases with and without the VO_x coating.

3.4.3 Impact of the coating on the current sharing behavior of REBCO tape

We first compare the evolution of the voltage across the middle section of the

REBCO tape (V7) before and after the coating with the REBCO tape remained at 77 K (Fig. 10). The voltage was measured from the Cu strip that was on top of the REBCO tape with and without the VO_x coating. When the current exceeds the critical current, the voltage increased exponentially following equation (1). The VO_x coating significantly reduced the voltage. For instance, at 110 A, the voltage decreased from 3 to 0.1 μV due to the coating. The high electrical resistance of the VO_x coating at 77 K effectively reduced the current sharing from the REBCO tape to the Cu strip and hence a lower voltage on the Cu strip was observed.

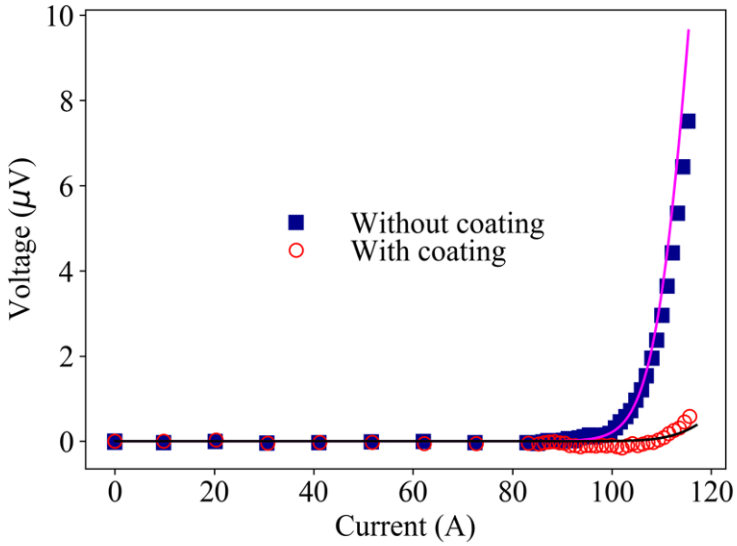

Fig. 10 Experiment and simulation results of the voltage of section V7 with and without VO_x coating, using a 1 mm thick and 3 mm wide Cu strip. Points: measurement. Lines: simulation.

Fig. 11 shows the voltage evolution measured from the Cu strip above the REBCO tapes with and without the VO_x coating. Also shown are the heater power and temperature. The voltage on the Cu strip was zero before firing the heater since the current was flowing through the superconducting REBCO tape at 77 K. The voltage started to rise a few seconds after the heater was on when the current shared from the REBCO tape into the Cu strip. All the voltages went back to zero when the REBCO tape cooled down.

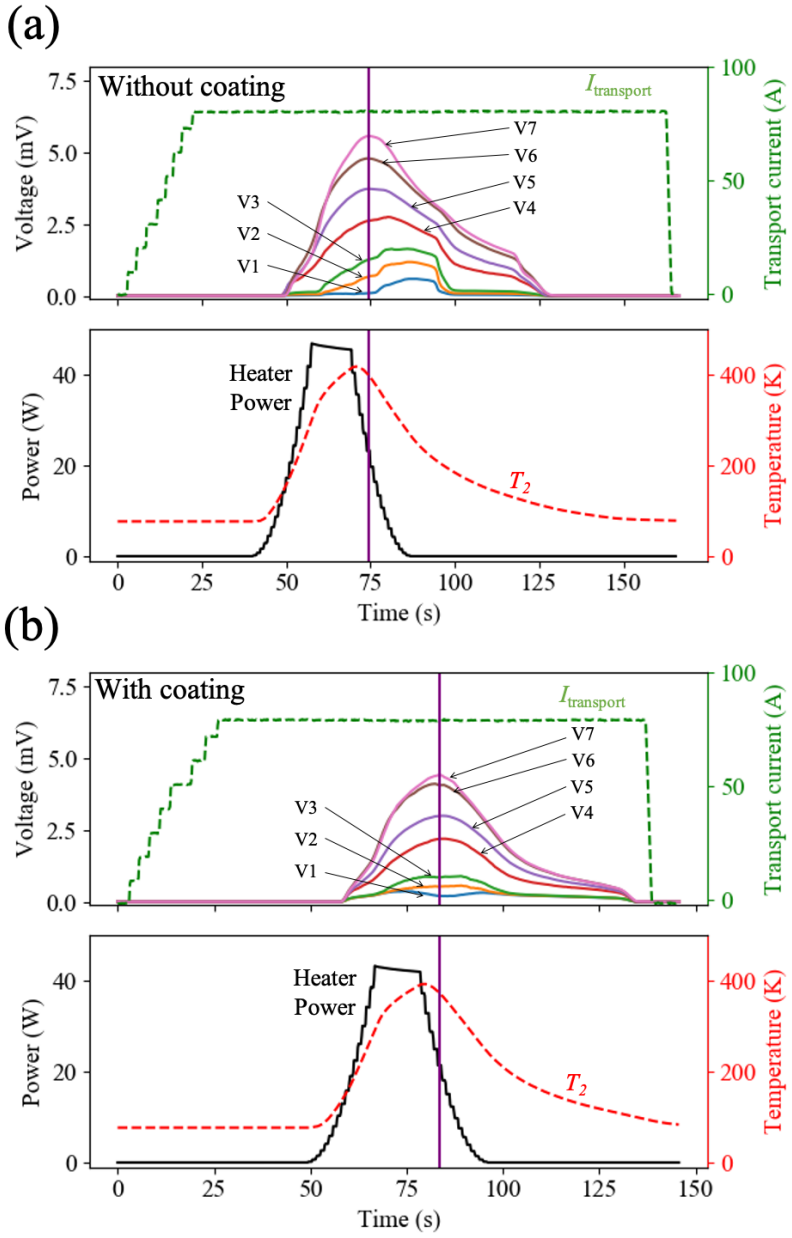

Fig. 11 The measured voltage evolution for all 12 sections of the Cu strip above the REBCO tape, the heater power and temperature after a constant transport current of 80 A was established. The heater H2 was near section V7. The Cu strip is 0.29 mm thick and 4 mm wide. (a) Without the VO_x coating and (b) with the VO_x coating. The vertical line at around 75 s in (a) and 80 s in (b) indicates the position we constructed the voltage profile for further comparison in Fig. 12.

To highlight the impact of VO_x coating, we constructed a voltage profile along the Cu strip by selecting the voltage across each section when the voltage across Section 7 reached its peak value as marked by the vertical line around 75 s in Fig. 11 (a). Fig. 12 compares the resulting voltage profiles with and without the VO_x coating. The voltages across each section decreased with the VO_x coating after a local hot spot

was introduced simulating a quench scenario.

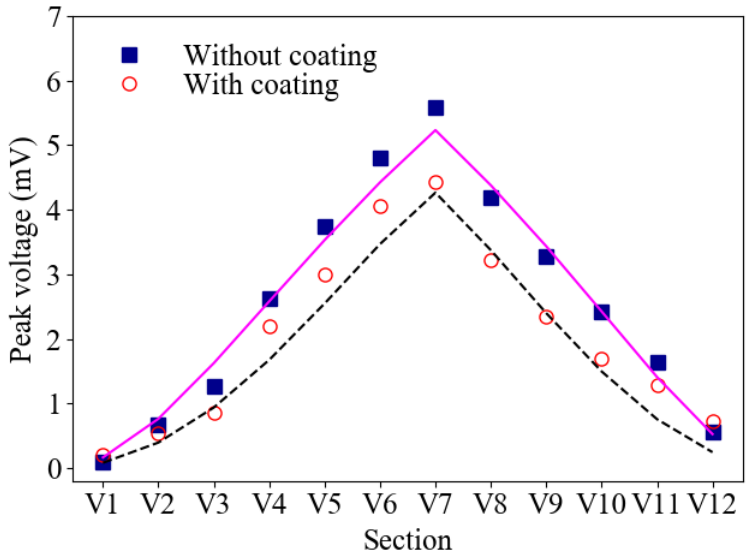

Fig. 12 Experimental and calculated spatial voltage profile along the REBCO tape when a local hot spot is induced in section V7. Points: measurement. Lines: simulation.

3.5 Analysis of the effect of VO_x coatings on the current sharing behavior based on the electric-circuit model

Using the parameters given in Table 1 (Appendix A), we first calculated the expected voltage rise during the current ramping at 77 K for the cases with and without the VO_x coating (section 3.4.3, Fig. 10). The calculated and measured voltage-current behavior agreed reasonably well (Fig. 10), confirming that the high electrical resistance of the VO_x coating at 77 K reduces the current sharing from the REBCO tape to the Cu strip compared to the cases without the coating. The agreement with the measured data also validates the circuit model.

To simulate the voltage distribution for the current sharing experiment due to a local hot spot (section 3.4.3, Fig. 12), we incorporated the temperature-dependent resistances in the circuit model. We assumed a linear temperature dependence for the VO_x coating resistivity based on the values of 1 Ω·cm at 300 K and 12 Ω·cm at 77 K. We note that the analysis here used a VO_x resistivity at 77 K that is lower than the one reported from the lap-joint measurement, because the voltage rise during the current ramping for this coated tape suggested a lower VO_x resistivity that was calculated

from fitting the voltage evolution with the VO_x coating resistance as fitting parameter. A lower coating thickness can explain the reduction of the resistivity.

The resulting temperature profiles for the cases with and without the coating based on the measured heater power are shown in Fig. 13. More details of the temperature profile and parameters used in the circuit model are summarized in Appendix B.

The calculated spatial voltage profiles are shown in Fig. 12. The calculation qualitatively agreed with the experimental results, indicating the circuit model reproduced the essential physics of experiments. The assumed uniform coating properties such as thickness and resistivity along the tape length and the simplified temperature profile used here may explain the differences between the measured and calculated voltage profiles.

With the validated model we can clearly discern the impact of the VO_x coating by comparing the current distribution in the REBCO layer (I_{HTS}), Cu stabilizer ($I_{stabilizer}$), and Cu strip (I_{strip}) based on the circuit simulation results (Fig. 13). At both ends of the REBCO tapes where the temperature is close to 100 K, the VO_x coating suppressed the current sharing. The current flowing in the Cu strip reduced from 32 A without the coating to 17 A with the coating. This is due to the higher resistance of the VO_x coating at the end sections with lower temperatures as they are away from the heater. This analysis result suggests that the VO_x coating can effectively suppress the eddy currents between the tapes during current ramping for REBCO cables and magnets.

When the temperature increased in the center sections of the REBCO tape after a heater-induced quench, the resistance of the VO_x coating decreased, allowing the current to share into the Cu strip at the heated sections (Fig. 13). The amount of current that shared into the Cu strip in sections V6 and V7 approached the case without the coating.

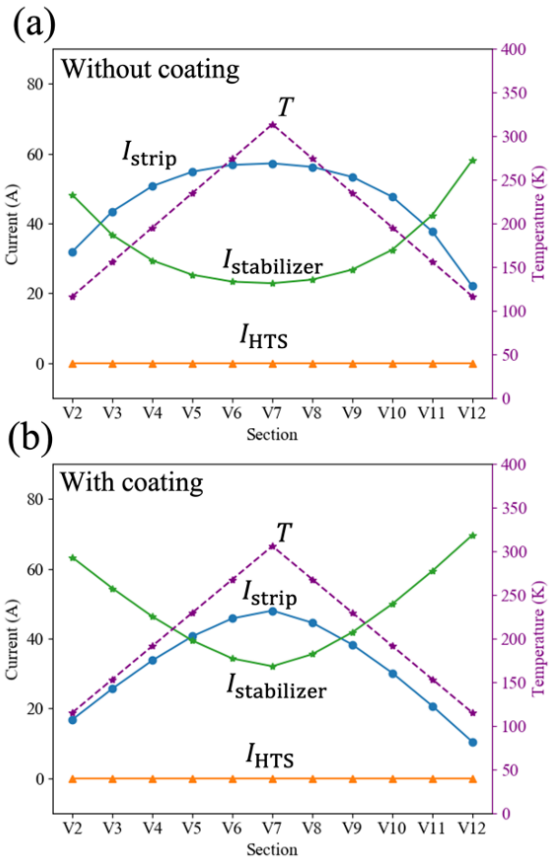

Fig. 13 Current distribution among the REBCO layer (I_{HTS}), stabilizer ($I_{stabilizer}$), and Cu strip (I_{strip}) (a) without the VO_x coating and (b) with the VO_x coating.

We expect a stronger impact on the current sharing with a higher resistivity ratio of the coating as one can achieve from single-crystal V_2O_3.[26] For instance, the current sharing will be further reduced at cold sections and enhanced at the heated sections. The analysis shown here considers the steady-state case. The sharp metal-insulator transition as expected from the single-crystal phase may also affect the dynamic current sharing behavior. Further optimization of the coating deposition process to achieve the desired resistivity range and transition behavior will be performed. Further demonstration of the impact of the VO_x coating in strong background magnetic fields and the development of optimal VO_x resistivity ranges for different REBCO cable and magnet applications are also planned.

4. Conclusions

Due to its negative temperature-dependence of the electrical resistivity, VO_x

coating on REBCO tapes was selected as a potential solution to suppress the undesired eddy currents during charging while enabling current sharing and self-protection during a superconducting-to-normal transition. As a first step to prove this concept and demonstrate the potential for REBCO cable and magnet applications, VO_x coatings were successfully deposited on REBCO tapes at different oxygen flow rates using a cathodic arc deposition process. The O/V ratios of the coating were determined by Rutherford Backscattering to be between 1.7 and 2.07. Raman spectrometry combined with XRD indicated that the coatings were X-ray amorphous but consisted of multiple phases of vanadium oxide with short-range crystalline ordering. The resistivity at room temperature (300 K) was highly sensitive to the oxygen flow rate used during deposition: it increased by four orders of magnitude when the oxygen flow increased by 8 sccm. The VO_x coatings showed orders of magnitude resistance drop when the temperature increased from 80 K to 300 K, which is necessary for potential application to regulate the current sharing behavior in REBCO cables and magnets. The resistivity of the VO_x coating deposited on commercial REBCO tapes was about 300 times higher at 77 K compared to the resistivity at 300 K based on a lap-joint measurement. More detailed characterization and development of the coating process to achieve consistently high resistivity ratio on long length REBCO tapes will be developed as a next step.

Current carrying capability of the REBCO tape was preserved with the developed coating process as evidenced by the negligible change of its critical current before and after the coating. Current sharing behavior at different scenarios were investigated for REBCO tapes with and without the VO_x coating, confirming the expected behavior of the VO_x coating.

The current sharing experiment and analysis based on a circuit model clearly showed that the VO_x coating has the potential to serve as a temperature-regulated self-switching medium between REBCO tapes to regulate current sharing behaviors: it can suppress the undesired current sharing, as an electrical insulator, at low temperature

and can allow, as an electrical conductor, current sharing between REBCO tapes when the temperature increases during a quench.

Acknowledgements

The work was supported by the Office of Science, Office of Fusion Energy Sciences, U.S. Department of Energy under Contract No. DE-AC02-05CH11231 and the Laboratory Directed Research and Development (LDRD) funding from the Lawrence Berkeley National Laboratory provided by the Director. Work at the Molecular Foundry was supported by the Office of Science, Office of Basic Energy Sciences, of the U.S. Department of Energy under Contract No. DE-AC02-05CH11231. Z. Yang acknowledges financial support from the China Scholarship Council, and A. Anders from the Free State of Saxony and the European Regional Development Fund (grant no. 100336119). The authors would like to thank Joe Wallig and Tak Katayanagi for their dedicated technical support, thank Dr. Yeonbae Lee for his help with RBS measurement, thank Prof. Peidong Yang and his student Minliang Lai for the XRD measurement, and thank Tevye Kuykendall at Molecular Foundry for his training about the Hall effect measurement.

References

1 G. Sun, X. Cao, S. Long, R. Li, and P. Jin, "Optical and electrical performance of thermochromic V_2O_3 thin film fabricated by magnetron sputtering." Applied Physics Letters **111,** 053901 (2017).

2 A. S. McLeod, E. van Heumen, J. G. Ramirez, S. Wang, T. Saerbeck, S. Guenon, M. Goldflam, L. Anderegg, P. Kelly, A. Mueller, M. K. Liu, I. K. Schuller, and D. N. Basov, "Nanotextured phase coexistence in the correlated insulator V_2O_3." Nature Physics **13,** 80 (2016).

3 T. J. Huffman, D. J. Lahneman, S. L. Wang, T. Slusar, B. J. Kim, H. T. Kim, and M. M. Qazilbash, "Highly repeatable nanoscale phase coexistence in vanadium dioxide films." Physical Review B **97**, 8 (2018).

4 G. Sun, X. Cao, X. Li, S. Bao, N. Li, M. Liang, A. Gloter, H. Gu, and P. Jin, "Low-temperature deposition of VO_2 films with high crystalline degree by embedding multilayered structure." Solar Energy Materials and Solar Cells **161,** 70 (2017).

5 K. Ran, W. Huang, Q. Shi, L. Tang, B. Peng, S. Liang, H. Zhu, and Z. Mao, "Freeze-drying induced nanocrystallization of VO_2 (M) with improved mid-infrared switching properties." Journal of Alloys and Compounds **728,** 1076 (2017).

6 Z. Liang, L. Zhao, W. Meng, C. Zhong, S. Wei, B. Dong, Z. Xu, L. Wan, and S. Wang, "Tungsten-doped vanadium dioxide thin films as smart windows with self-cleaning and energy-saving functions." Journal of Alloys and Compounds **694,** 124 (2017).

7 A. Aijaz, Y.-X. Ji, J. Montero, G. A. Niklasson, C. G. Granqvist, and T. Kubart, "Low-temperature synthesis of thermochromic vanadium dioxide thin films by reactive high power impulse magnetron sputtering." Solar Energy Materials and Solar Cells **149,** 137 (2016).

8 J. Lee, D. Lee, S. J. Cho, J. H. Seo, D. Liu, C. B. Eom, and Z. Ma, "Epitaxial VO_2 thin film-based radio-frequency switches with thermal activation." Applied Physics Letters **111,** 063110 (2017).

9 C. Wu, F. Feng, and Y. Xie, "Design of vanadium oxide structures with controllable electrical properties for energy applications." Chemical Society Reviews **42,** 5157 (2013).

10 B. T. Liu, X. M. Shi, X. Y. Lang, L. Gu, Z. Wen, M. Zhao, and Q. Jiang, "Extraordinary pseudocapacitive energy storage triggered by phase transformation in hierarchical vanadium oxides." Nature communications **9,** 1375 (2018).

11 J. S. Brockman, L. Gao, B. Hughes, C. T. Rettner, M. G. Samant, K. P. Roche, and S. S. Parkin, "Subnanosecond incubation times for electric-field-induced metallization of a correlated electron oxide." Nature nanotechnology **9,** 453 (2014).

12 A. Gerbershagen, C. Calzolaio, D. Meer, S. Sanfilippo, and M. Schippers, "The advantages and challenges of superconducting magnets in particle therapy." Superconductor Science and Technology **29,** 083001 (2016).

13 H. Maeda and Y. Yanagisawa, "Recent Developments in High-Temperature Superconducting Magnet Technology." IEEE Transactions on Applied Superconductivity **24,** 1 (2014).

14 See https://escholarship.org/uc/item/5178744r for the US Magnet Development Program Plan, Lawrence Berkeley National Laboratory report #LBNL-1006046

15 S. C. Ritz, "Building for Discovery: Strategic Plan for U.S. Particle Physics in the Global

Context. Report of the Particle Physics Project Prioritization Panel (P5)," HEPAP Subcommittee (2014).

16 L. Rossi, A. Badel, M. Bajko, A. Ballarino, L. Bottura, M. M. J. Dhallé, M. Durante, P. Fazilleau, J. Fleiter, W. Goldacker, E. Härö, A. Kario, G. Kirby, C. Lorin, J. v. Nugteren, G. d. Rijk, T. Salmi, C. Senatore, A. Stenvall, P. Tixador, A. Usoskin, G. Volpini, Y. Yang, and N. Zangenberg, "The EuCARD-2 future magnets European collaboration for accelerator-quality HTS magnets." IEEE Transactions on Applied Superconductivity **25**, 1 (2015).

17 B. N. Sorbom, J. Ball, T. R. Palmer, F. J. Mangiarotti, J. M. Sierchio, P. Bonoli, C. Kasten, D. A. Sutherland, H. S. Barnard, C. B. Haakonsen, J. Goh, C. Sung, and D. G. Whyte, "ARC: A compact, high-field, fusion nuclear science facility and demonstration power plant with demountable magnets" Fusion Engineering and Design **100**, 378 (2015).

18 A. Bergen, R. Andersen, M. Bauer, H. Boy, M. T. Brake, P. Brutsaert, C. Bührer, M. Dhallé, J. Hansen, H. ten Kate, J. Kellers, J. Krause, E. Krooshoop, C. Kruse, H. Kylling, M. Pilas, H. Pütz, A. Rebsdorf, M. Reckhard, E. Seitz, H. Springer, X. Song, N. Tzabar, S. Wessel, J. Wiezoreck, T. Winkler, and K. Yagotyntsev, "Design and in-field testing of the world's first ReBCO rotor for a 3.6 MW wind generato." Superconductor Science and Technology **32,** 1 (2020).

19 X. Song, C. Buhrer, P. Brutsaert, A. Ammar, J. Krause, A. Bergen, T. Winkler, M. Dhalle, J. Hansen, A. V. Rebsdorf, S. Wessel, M. t. Brake, M. Bauer, J. Kellers, J. Wiezoreck, H. Putz, H. Kylling, H. Boy, and E. Seitz, "Ground Testing of the World's First MW-Class Direct-Drive Superconducting Wind Turbine Generator." IEEE Transactions on Energy Conversion, **35**, 757 (2019).

20 M. N. Wilson, "Superconducting Magnets," Oxford University Press. (1984).

21 Y. Iwasa, "Case studies in superconducting magnets: design and operational issues." Springer Science & Business Media, (2009).

22 S. Hahn, D. K. Park, J. Bascuñán, and Y. Iwasa, "HTS pancake coils without turn-to-turn insulation." IEEE transactions on applied superconductivity. **21**, 1592 (2011).

23 Y. Wang, H. Song, W. Yuan, Z. Jin, and Z. Hong, "Ramping turn-to-turn loss and magnetization loss of a No-Insulation (RE) $Ba_2Cu_3O_x$ high temperature superconductor pancake coil." Journal of Applied Physics. **121,** 113903 (2017).

24 X. Wang, T. Wang, E. Nakada, A. Ishiyama, R. Itoh, and S. Noguchi, "Charging behavior in no-insulation REBCO pancake coils." IEEE Transactions on Applied Superconductivity **25,** 1 (2015).

25 Y. Suetomi, K. Yanagisawa, H. Nakagome, M. Hamada, H. Maeda, and Y. Yanagisawa, "Mechanism of notable difference in the field delay times of no-insulation layer-wound and pancake-wound REBCO coils." Superconductor Science and Technology **29,** 105002 (2016).

26 J. Kim, S. Yoon, K. Cheon, K. H. Shin, S. Hahn, D. L. Kim, S. Lee, H. Lee, and S. Moon, "Effect of resistive metal cladding of HTS tape on the characteristic of no-insulation coil." IEEE Transactions on Applied Superconductivity **26**, 4 (2016).

27 J. Lu, J. Levitan, D. N. Mcrae, and W. Robert, "Contact resistance between two REBCO tapes: The effects of cyclic loading and surface coating." Superconductor Science and Technology, **31**, 8 (2018).

28 H. W. Kim, Y. S. Jo, S. W. Kim, D. W. Ha, R. K. Ko, D. Kim, and J. Hur, "Enhancement of 2G HTS coil stability with V_2O_3 and perforated HTS wire." IEEE Transactions on Applied Superconductivity **28,** 1 (2018).

29 H. W. Kim, J. Hur, S. W. Kim, S. B. Kim, R. K. Ko, D. W. Ha, H. M. Kim, J. H. Joo, and Y. S. Jo, "Improvement in stability and operating characteristics of HTS coil using MIT material." IEEE Transactions on Applied Superconductivity **27,** 1 (2017).

30 J. A. J. Rupp, M. Querre, A. Kindsmuller, M. P. Besland, E. Janod, R. Dittmann, R. Waser, and D. J. Wouters, "Different threshold and bipolar resistive switching mechanisms in reactively sputtered amorphous undoped and Cr-doped vanadium oxide thin films." Journal of Applied Physics **123,** 044502 (2018).

31 J. Sakai, M. Bavencoffe, B. Negulescu, P. Limelette, J. Wolfman, A. Tateyama, and H. Funakubo, "Strain-induced resistance change in V_2O_3 films on piezoelectric ceramic disks." Journal of Applied Physics **125,** 115102 (2019).

32 E. B. Thorsteinsson, S. Shayestehaminzadeh, and U. B. Arnalds, "Tuning metal-insulator transitions in epitaxial V_2O_3 thin films." Applied Physics Letters **112,** 161902 (2018).

33 A. Anders, Cathodic Arcs: From Fractal Spots to Energetic Condensation. Springer New York, 2008.

34 see http://www.superpower-inc.com/system/files/SP_2G+Wire+Spec+Sheet_for+web_2012FEC_v2_1.pdf for information about SuperPower REBCO-based 2G HTS wire specifications.

35 L. W. Nagel and D. O Pederson, SPICE (Simulation Program with Integrated Circuit Emphasis), Univ. of California, Berkeley, Electronics Research Laboratory (1973).

36 A. C. Araujo Martínez, Q. Ji, S. O. Prestemon, X. Wang and G. H. I. Maury Cuna, "An Electric-Circuit Model on the Inter-Tape Contact Resistance and Current Sharing for REBCO Cable and Magnet Applications." IEEE Transactions on Applied Superconductivity, **30**, 1 (2020).

37 J. Lu, R. Goddard, K. Han, and S. Hahn, "Contact resistance between two REBCO tapes under load and load cycles," Superconductor Science and Technology. 30, 045005 (2017).

38 X. B. Chen, J. H. Shin, H. T. Kim, and Y. S. Lim, "Raman analyses of co-phasing and hysteresis behaviors in V_2O_3 thin film." Journal of Raman Spectroscopy **43,** 2025 (2012).

39 S. H. Zhang, J. Fu, Q. C. Su, L. P. Wu, and X. J. Li, "In Situ Characterization on Thermal Transitions of VO_2 (B): Toward VO_2 (R) and V_2O_3." Rare Metal Materials and Engineering **45,** 1374 (2016).

40 A. J. Littlejohn, Y. Yang, Z. Lu, E. Shin, K. Pan, G. Subramanyam, V. Vasilyev, K. Leedy, T. Quach, T. M. Lu, and G. C. Wang, "Naturally formed ultrathin V_2O_5 heteroepitaxial layer on VO_2/sapphire (001) film." Applied Surface Science **419,** 365 (2017).

41 R. Baddour-Hadjean, C. Navone, and J. P. Pereira-Ramos, "In situ Raman microspectrometry investigation of electrochemical lithium intercalation into sputtered crystalline V_2O_5 thin films." Electrochimica Acta **54,** 6674 (2009).

42 R. Baddour-Hadjean, J. P. Pereira-Ramos, C. Navone, and M. Smirnov, "Raman microspectrometry study of electrochemical lithium intercalation into sputtered crystalline V_2O_5 thin films." Chemistry of Materials **20,** 1916 (2008).

43 D. Vernardou, D. Louloudakis, E. Spanakis, N. Katsarakis, and E. Koudoumas, "Thermochromic amorphous VO_2 coatings grown by APCVD using a single-precursor." Solar Energy Materials and Solar Cells **128,** 36 (2014).

44 D. P. Zhang, M. D. Zhu, Y. Liu, K. Yang, G.X. Liang, Z. H. Zheng, X. M. Cai, and P. Fan, "High performance VO_2 thin films growth by DC magnetron sputtering at low temperature for smart energy efficient window application" Journal of Alloys and Compounds **659,** 198 (2016).

45 G. A. Levin, W. A. Jones, K. A. Novak, and P. N. Barnes, "The effects of superconductor–stabilizer interfacial resistance on quenching of a pancake coil made out of coated conductor." Superconductor Science and Technology **24,** 035015 (2011).

Appendix A. Parameters for the circuit analysis in Fig. 10

Table 1 gives the electric circuit parameters used for the analysis shown in Fig. 10. The resistances were calculated based on the resistivities at 77 K. For the VO_x coating the resistivity used was 300 Ω·cm. For copper, we used 0.2 μΩ·cm.[45] The tape I_c and n were set to 95 A and 32 from the measurements.

Table 1. Parameters used in the circuit model at 77 K for Fig. 10.

	Length (mm)	Width (mm)	Thickness (mm)	Resistance (Ω)
Cu strip	6	3	1	4×10^{-6}
VO_x longitudinal	6	4	0.5×10^{-3}	9×10^{6}
VO_x transverse	0.5×10^{-3}	6	4	62.5×10^{-3}
Cu stabilizer	6	4	4×10^{-2}	0.75×10^{-4}

Appendix B. Parameters for the circuit analysis in Figs. 12 and 13

The analytical temperature profiles were calculated assuming steady state attained only by conduction through the HTS tape and Cu strip from a point heater at the center of the REBCO tape towards the cold ends which is given by

$$\frac{\partial T}{\partial x} = \frac{P_{avg}}{2K_{Cu}}$$

where T is temperature, x is the distance from the heater H2, P_{avg} is the time-averaged power from the heater and K_{Cu} is the thermal conductivity of copper. Since the Cu strip and REBCO tape are thin, we further assumed they have the same temperature. Solving for a simplified linear temperature profile with the peak at section V7 and 77 K at both ends of the tape, the peak temperature is given by

$$T_7 = \frac{P_{avg} \times L_{V10-V7}}{2 \times w \times t \times K_{Cu}} + 77$$

where $L_{V10\text{-}V7}$ gives the distance between sections V10 and V7, w is width of Cu strip and REBCO tape, and t is total thickness of the REBCO tape and the Cu strip. Here a temperature-averaged Cu thermal conductivity of 450 $Wm^{-1}K^{-1}$ is used. We also estimated the temperature profile based on the measured resistance of the Cu strip assuming all the current flows into the Cu strip once the REBCO tape starts quenching. The resulting peak temperature and the temperature profile are consistent with the analytic results.

The details of the electric-circuit model used to simulate the current sharing experiment with a local hot spot (Figs. 12 and 13) are shown in Fig. 14. The resistances of the Cu stabilizer ($R_{stabilizer}$), Cu strip (R_{strip}), and the VO_x transverse coating resistance ($R_{coating}$) for each section were calculated based on the Cu and VO_x resistivity for the given analytical temperature profile. The contact resistances ($R_{contact}$) along the tape sections were considered constant. The I_c values of the voltage sources were set to zero for all sections with temperature higher than 90 K. For section V1,

assumed to be at 77 K, the I_c was 98 A determined from the measured tape. The n value for all sections was 33.2.

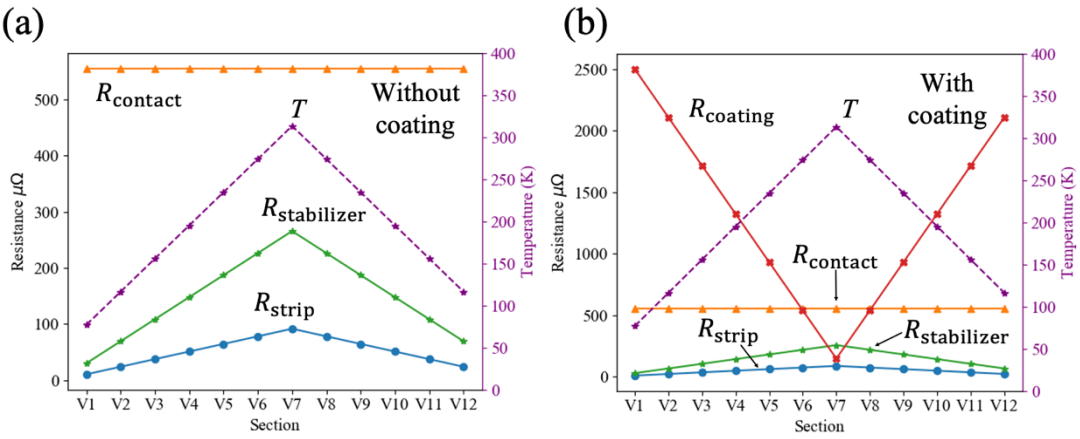

Fig. 14 Resistance values of the electric-circuit model given the analytical temperature profile (a) without VO_x coating and (b) with coating.

Data Availability Statement

The data that support the findings of this study are available from the corresponding author upon reasonable request.